Monte Carlo simulations of magnetization state of ellipsoidal CoCu particles in disordered self-assembled arrays

V.Z.C. Paes[b)] and J. Varalda
Departamento de Física, Universidade Federal do Paraná, 81531-990, Curitiba, PR, Brazil

P. Schio
Departamento de Física, Universidade Federal de São Carlos, 13565-905 São Carlos, SP, Brazil

J.T. Matsushima
Laboratório Associado de Sensores e Materiais, Instituto Nacional de Pesquisas Espaciais, CEP 12227-010, São José dos Campos, SP, Brazil

E.C. Pereira
Departamento de Química, Universidade Federal de São Carlos, 13565-905 São Carlos, SP, Brazil

A.J.A. de Oliveira
Departamento de Física, Universidade Federal de São Carlos, 13565-905 São Carlos, SP, Brazil

D.H. Mosca[a)]
Departamento de Física, Universidade Federal do Paraná, 81531-990, Curitiba, PR, Brazil

(Received 9 August 2015; accepted 13 April 2016)

Monte Carlo (MC) simulations of the magnetization states of disordered self-assembled arrays of particles consisting of $Co_{87}Cu_{13}$ alloy are investigated. The assemblies of magnetic particles with ellipsoidal shapes and volumes ranging from 5 to 50 μm^3 exhibit densities of about 3×10^6 particles per mm^2. Magnetization was obtained in the framework of Stoner–Wohlfarth model extended to include phenomenological contributions of second-order magnetic anisotropy and coercivity mechanism with distinct configuration of easy axes of magnetization. MC simulations for assemblies containing no more than 100 particles with negligible magnetic interaction between each other and exhibiting saturation magnetization and magnetic anisotropy constant values close to those found for cobalt in bulk are in good agreement with experimental results. We evaluate and validate our computational modeling using samples having particles with different sizes and different angular distributions of the easy axis of magnetization. A simple numerical approach with minimum of parameters was used to take into account the coercive fields of the samples. Reasonable simulation results are generated based on realistic size distributions and angular distributions of easy axis of magnetization.

PACS numbers: 75.30.Gw,75.60-d,75.70-i

I. INTRODUCTION

Systems of magnetic particles in the micro and nanometric size range exhibit a wide variety of experimental behavior[1,2] with important technological uses mainly in the magnetic data storage technologies[3–5] and in medicine.[6] The Stoner–Wohlfarth (SW) model[7] describes the major hysteresis loop for an isotropic system of randomly oriented and identical single-particles, but it is mostly used to study dilute noninteracting systems of randomly aligned single-domain particles presenting uniaxial anisotropy. Only uniaxial anisotropy and the Zeeman energy are considered, resulting in a coherent magnetization rotation mechanism. SW model is also a reasonable first-order approach to describe the magnetization curves of polycrystalline materials consisting of an assembly of small noninteracting particles with uniaxial anisotropy and for a wide range of particle sizes. Nevertheless, in dense systems the mutual interactions between the magnetic particles is commonly assumed to play a dominant role. A wide variety of magnetic responses (magnetization and demagnetization processes, magnetization reversal and switching, time relaxation, blocking phenomena, among others) takes place for dense assemblies of fine (sizes from a few tens of nanometers to several tens of micrometers) ferromagnetic particles assuming coherent magnetization rotation and nucleation within particles with uniaxial anisotropy. Further features like particle shapes, array geometries, dipole–dipole interactions between particles

Contributing Editor: Yang-T. Cheng
[a)]Address all correspondence to this author.
e-mail: mosca@fisica.ufpr.br
[b)]Present address: Instituto de Física, Universidade Federal do Rio Grande do Sul, Av. Bento Gonçalves, 9500 – Caixa Postal 15051 – CEP 91501-970 – Porto Alegre, RS, Brazil.
DOI: 10.1557/jmr.2016.173

affect significantly the dynamic and static magnetic properties.[8–14] In contrast to dilute systems, dense systems are not completely understood even in patterned arrays of neatly coupled objects. The design of dense magnetic systems microscaled and nanoscaled is a key issue for future applications to high-density magnetic recording. Mean-field approximation and Monte Carlo (MC) simulations[12,15] are often used to study dense systems. Both approaches have been made to improve the accuracy of the magnetic properties simulation of real particle systems with irregular shape, nonuniform size, and disordered spatial distribution of easy axes of magnetization with or without dipolar interaction.[16] However, the simplicity of the micromagnetics modeling and the challenge to compute properly remain important biases in such approaches.

In this work, we investigate dense systems of magnetic particles of CoCu alloy with nonuniform sizes and irregular distances, which have easy axis distributions mostly oriented either parallel or perpendicular to the film plane. MC simulations of the magnetization of dense and disordered assemblies of particles were performed in the SW model framework and compared with experimental data.

II. EXPERIMENTAL DETAILS AND MEASUREMENTS

Electrodeposits of $Co_{87}Cu_{13}$ alloys were obtained on polished copper foil substrates from solutions containing 0.5 M $CoSO_4{\cdot}7H_2O$, 0.05 M $CuSO_4{\cdot}6H_2O$, and 1.0 M Na_2SO_4 using a chrono-amperometric method with cathodic potential at a different values of −1.0 V and −1.1 V versus saturated calomel electrode (SCE) applied during 90 s.[17] The effective thickness of the films is approximately 0.7 μm. This value is consistent with observed saturation magnetization and mass evaluations using electrochemical quartz crystal microbalance. According to scanning electron microscopy (SEM) analyses performed using a JSM-5800 microscope (JEOL Ltd., Tokyo, Japan) operating at 25 kV, these electrodeposits consist of dense assemblies of $Co_{87}Cu_{13}$ grains. SEM images shown in Figs. 1(a) and 1(b) reveal different assemblies of elongated particles for Sample A electrodeposited at a potential of −1.0 V and Sample B electrodeposited at a potential of −1.1 V. Sizes and separations of the grains are variable in the Sample A. Besides, the elongated axis of each grain is mostly aligned in the film plane with a broad in-plane angular distribution. In Sample B, the sizes and separations of the grains are also variable, but the elongated axis of each grain tends to align parallel to the normal direction of the film with a small out-of-plane angular distribution. In this case, the different choices of the deposition potentials in the flank of the nucleation wave lead to electrodeposits with quite distinct distribution of orientations of grains and alloys with almost the same stoichiometry of

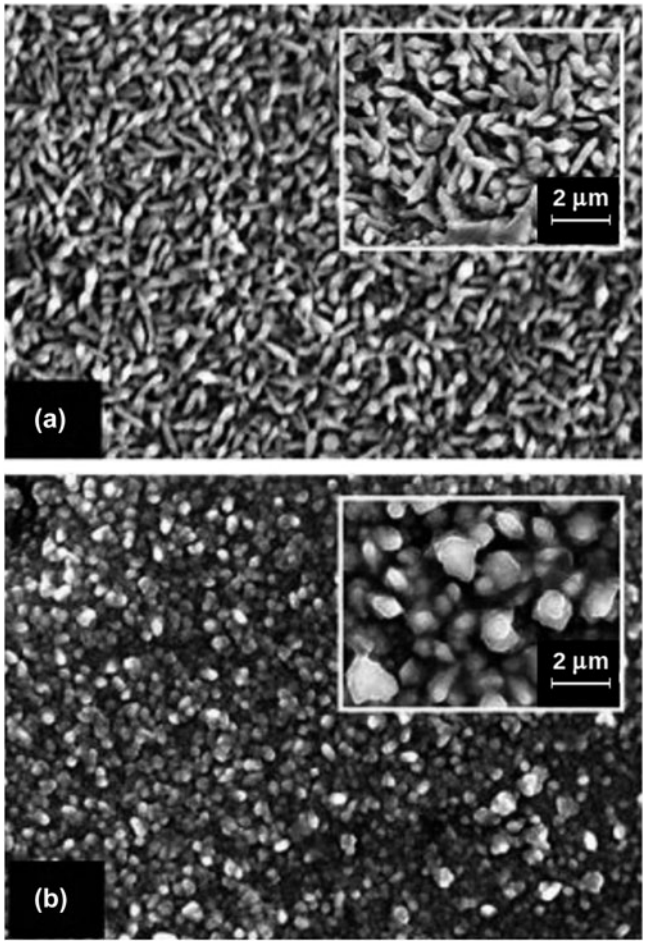

FIG. 1. SEM images obtained for (a) Sample A and (b) Sample B prepared at deposition potentials of −1.0 and −1.1 V versus SCE, respectively. The main pictures are at 1300× magnification.

$Co_{87}Cu_{13}$. Similarly to cobalt films electrodeposited on copper substrates, these films display a mixture of face-centered cubic and hexagonal close-packed phase, whose proportion and grain morphology depend on the deposition potential.[18] We investigate in the present work the magnetic behavior of the electrodeposits, whose morphology presents distinct assemblies of grains (hereafter called particles).

Magnetic hysteresis (M–H) loops measured at room temperature for these two samples using a vibrating sample magnetometer (EG&G model VSM-4500, Oak Ridge, Tennessee) are shown in Figs. 2(a) and 2(b). Magnetization M is normalized to the saturation magnetization M_S, whereas the magnetic field H is applied along different directions relative to the film plane. Clearly, M–H loops depend on the angle of the applied magnetic field relative to film plane and angular distributions of the elongated axis of the particles significantly affect the magnetization processes and the magnetic anisotropy. Different M–H loops are found with magnetic fields applied along different orientations with respect to the

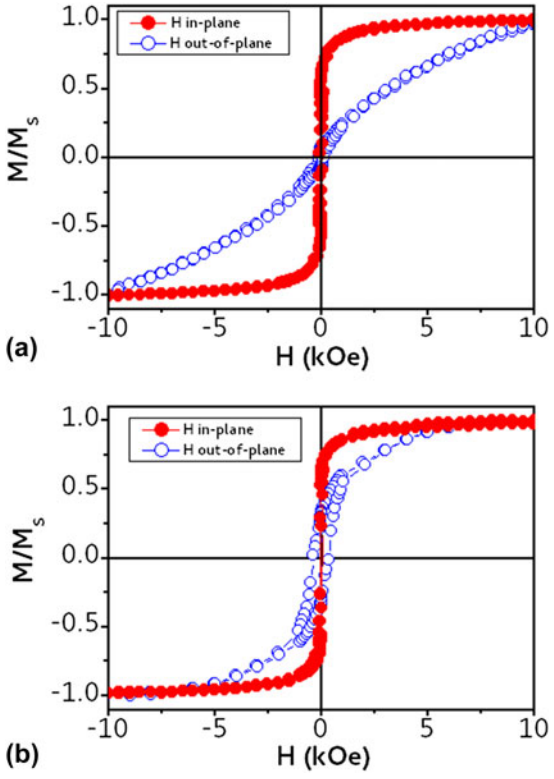

FIG. 2. *M–H* loops measured at room temperature for (a) Sample A and (b) Sample B prepared at deposition potentials of −1.0 and −1.1 V versus SCE, respectively.

film plane. Comparatively to Sample A, which consists of particles with elongated axis distributed in the film plane, Sample B with particles having elongated axes mostly orientated out of the film plane exhibits a magnetization with stronger out-of-plane component. We will focus our attention on the *M–H* loops of these assemblies of particles in the cases of magnetic field applied perpendicular and parallel to the film plane.

III. SIMULATION DETAILS AND DISCUSSION

Let us now address our physical assumptions to built a consistent model and perform computational simulations of the *M–H* loops of these magnetic particle systems. We assume that the samples can be described by systems of ellipsoidal particles for Sample A and half-ellipsoidal particles for Sample B, as shown in Figs. 3(a) and 3(b). The volume of the particles ranges from 5 to 25 μm^3 for Sample A and 3 to 50 μm^3 for Sample B. A density of 3×10^6 particles per mm^2 is estimated for sample areas of 20 mm^2 which are used in magnetic measurements. It is assumed that the magnetic moments inside each particle are quasihomogeneously magnetized and only the total magnetization direction along its easy axis changes from a particle to the next. Every particle i consists of a single magnetic domain in the sense that its atomic magnetic moments rotates coherently and their total magnetic moment μ_i is given by constant absolute value $|\mu_i| = M_S V_i$. Here, V_i is the volume of particle i and M_S is the saturation magnetization with value of $M_S = 1100$ emu/cm^3, that is supposed to be independent of the particle volume. The magnetization of all particles can rotate freely in any direction when one external field is applied because the domain wall is not considered. This model represents the reversible and the irreversible magnetization process as well, since the abrupt changes in the orientation of the magnetization mimic the Barkhausen jumps. In the standard SW model, these jumps can appear when the magnetic field intensity crosses the asteroid shape from inside to outside.[19]

The magnetic anisotropy of each particle is expected to be similar to that of the pure cobalt. Whereas, the first-order magnetocrystalline constant denoted by K_1 is assumed to be very close to bulk value, K_2 is free to vary from sample to sample. The shape anisotropy also contributes to the effective values for K_1 and K_2 constants.[20] The easy axes of each particle are spatially distributed at random in each sample. However, there are experimental evidences indicating preferential angular distributions of the elongated axes either parallel or perpendicular to the normal direction of the film plane, as observed in Figs. 1(a) and 1(b). These axes are assumed as easy axes of magnetization. A small number (no more than 100) of particles were considered to obtain a realistic simulation of the *M–H* loops. The volumes V_i and orientation of easy axes of magnetization (major axis of particle) used as inputs for the calculations. These parameters were independently extracted from the experimental data shown in Figs. 1(a) and 1(b). For sake of simplicity, we disregard the influence of interparticle dipole–dipole interactions on the global magnetization. The total number of particles was progressively increased from 1 to 100. Although numerical simulation of the magnetization distribution in a system composed of few noninteracting magnetic particles can be seen as a simplified approach, it is striking to realize that a quite good agreement is obtained between simulated curves and experimental results using no more than 100 particles.

The total magnetic energy E_i of each particle i is considered by the sum of three contributions: Zeeman field energy, magnetic anisotropy terms of energy (either due to the shape or the crystalline structure of the particle), and domain nucleation energy. Thus, the density of magnetic free energy for each particle can be written as[21–25]:

$$E_i = -H \cdot M_S + K_1 \sin^2(\theta_i - \theta_{oi}) + K_2 \sin^4(\theta_i - \theta_{oi}) + E_d \quad , \tag{1}$$

where H is the applied magnetic field, M_S is the saturation magnetization, K_1 and K_2 are the effective

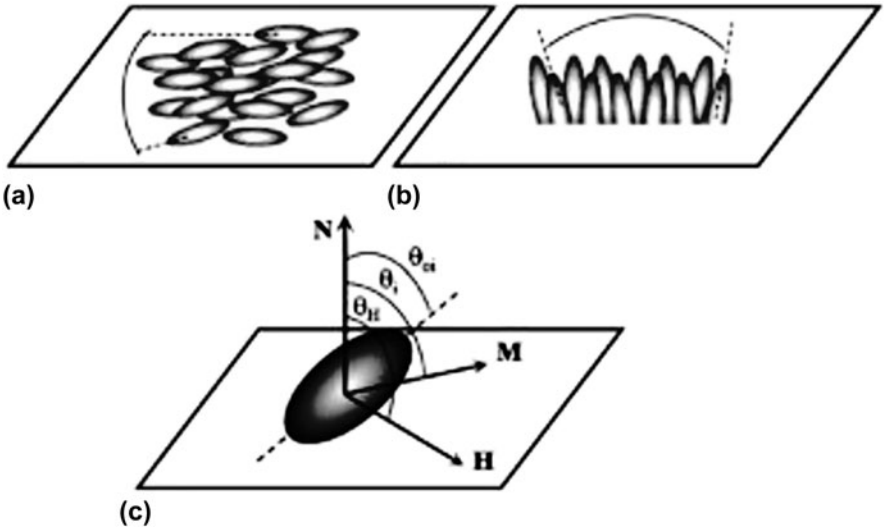

FIG. 3. Schematic illustration of the assemblies of (a) elongated ellipsoids and (b) half-ellipsoids used to model the morphology of the Samples A and B, respectively. (c) Convention used to define the angular coordinates between film normal N and major axis (dashed line) of an ellipsoidal particle, magnetization M and applied field H.

first- and second-order anisotropy constants, that include a priori magnetocrystalline anisotropy constants added to shape anisotropy constants,[22] θ_i is the polar angle that the magnetic moment of i-th particle makes with the film normal [see Fig. 3(a)], θ_{oi} is the polar angle that the easy axis of the i-th particle makes to the film normal, and E_d is an additional contribution which takes into account the domain nucleation energy which is described below.

In Sample A, the particles are assumed as ellipsoids with variable sizes, whereas in Sample B the particles are taken as half-ellipsoids of variable sizes. Initially, the values of θ_{oi} are randomly generated by taking random initial values. This allows the determination of the angular distribution of the major axis of the particles from the best agreement between simulated and experimental M–H loops. For simplicity, the exchange interaction between particles is disregarded.[23] These drastic assumptions are of importance to test the validity of our present calculations by comparison with experimental results.

To simulate the M–H loops for a magnetic field applied along the hard axis, we must take into account that there are maybe some particles with their easy axes oriented parallel to the direction of the applied field. This point is important to solve the so-called Brown paradox which states that, in general, the experimental coercivity is much lower than predicted by the SW model. Based on previous works,[24,25] an additional energy contribution is used only for the particles with their easy axes orientated parallel to the applied magnetic field which is given by:

$$E_d = -M_S H_{oi} \cos\left(\theta_{i(n)} - \theta_{i(n-1)}\right) \quad , \qquad (2a)$$

where H_{oi} are free parameters that control the coercive field H_c and $\theta_{i(n)}$ is the angle of the n-th iteration of the calculation of the magnetization contribution for the i-th particle. The H_o parameter can be varied from one direction of application of the field to another due to the demagnetizing factors[26] which also delimit the values of H_o parameters. This approach leads to quite good simulation results. The distribution of the coercive fields from particle to particle prevents the deduction of a precise evaluation of their collective behavior. However, when the particles have the easy-axis aligned along the out-of-plane direction, we must use instead of Eq. (2a), the following equation:

$$E_d = -M_S H_{oi} \sin\left(\theta_{i(n)} - \theta_{i(n-1)}\right) \quad , \qquad (2b)$$

here, the energy minimization procedure to obtain the magnetization needs a more careful analysis than in SW-like models. Considering that the magnetization value must lead to a stable equilibrium, it should be closer to its previous value. Thus, the energy minimization procedure is performed and compared to the calculated magnetization value obtained for an applied field which is slightly different from the previous one. However, the exact calculation of the equilibrium positions of the magnetization for a given field leads to a large number of coupled equations and free parameters. Thus, it was adopted the following procedure. For a given direction of application of the magnetic field, the n-th particle presents easy-axis along or near such a direction in accordance to Figs. 1(a) and 1(b). To minimize the number of parameters is imposed a criterion that H_o values are constant for a given field direction; i.e., there is no angular dependence of this term relative to the applied field direction.

To validate the model were simulate the M–H loops measured at room temperature for Sample A and Sample

B with magnetic field applied parallel and perpendicular to film plane. MC simulations were used to calculate the magnetization of the particles in the applied magnetic field for each easy axis configuration of magnetization. The representative number of particles was increased up to 100 to obtain reasonable simulations of the magnetic hysteresis loops. In these simulations considering assemblies of $N \times N$ particles with $N = 10$ were left free to vary only with the values of second-order anisotropy constant, K_2, and the parameter that controls the coercivity for the assembly of particles, namely H_o. All others parameters were kept fixed, independent of the orientation of the applied magnetic field relative to film plane. MC simulations are shown in Fig. 4 only with $N = 10$. Simulated and measured M–H loops for magnetic field applied along the in-plane easy axes of magnetization for Sample A and Sample B are shown in Figs. 4(a) and 4(b), respectively. A good agreement is obtained between simulations and experimental results for both samples, including reasonable values for coercivities and remanences. Our simulations of the M–H loops with magnetic field applied along the hard axis of magnetization of Sample A and Sample B are shown in Figs. 4(c) and 4(d), respectively. Again, these simulations are in good agreement with experimental data. The values used in these simulations are given in Table I. For magnetic field applied in the easy axis, both M_S and K_1 are the same for Samples A and B. Different values for K_2 and H_oM_S were used to obtain the simulations of hysteresis loops observed for Sample A and Sample B. The same M_S and K_1 values were used for magnetic field applied along the hard axis. Again, the hysteresis loops for Sample A and Sample B are better reproduced using different values for K_2 and H_oM_S. Such changes in K_2 and H_o are expected because the contribution of shape anisotropy is included in the K_2 anisotropy constant and H_o values. These values depend on the average major axis of the particles along the applied field direction.

According to the simulations for Sample A, the easy axes of magnetization are aligned parallel to the film normal for 6% of the particles. For the remaining 94% of the particles, the easy axes of magnetization exhibit azimuthal angles randomly oriented in the film plane and polar angles ranging in between 45° and 90° (in the film plane). For Sample B, the simulations correspond to 40% of the particles with easy axes of magnetization aligned along the film normal and the remainder particles present a distribution of the easy axis of magnetization centered at 0° with an angular opening of 45° and a width of approximately 26°. These features are in good agreement with the features of SEM images shown in Figs. 1(a) and 1(b). Therefore, reasonable simulation results are generated using realistic size distributions and angular distributions of easy axes of magnetization.

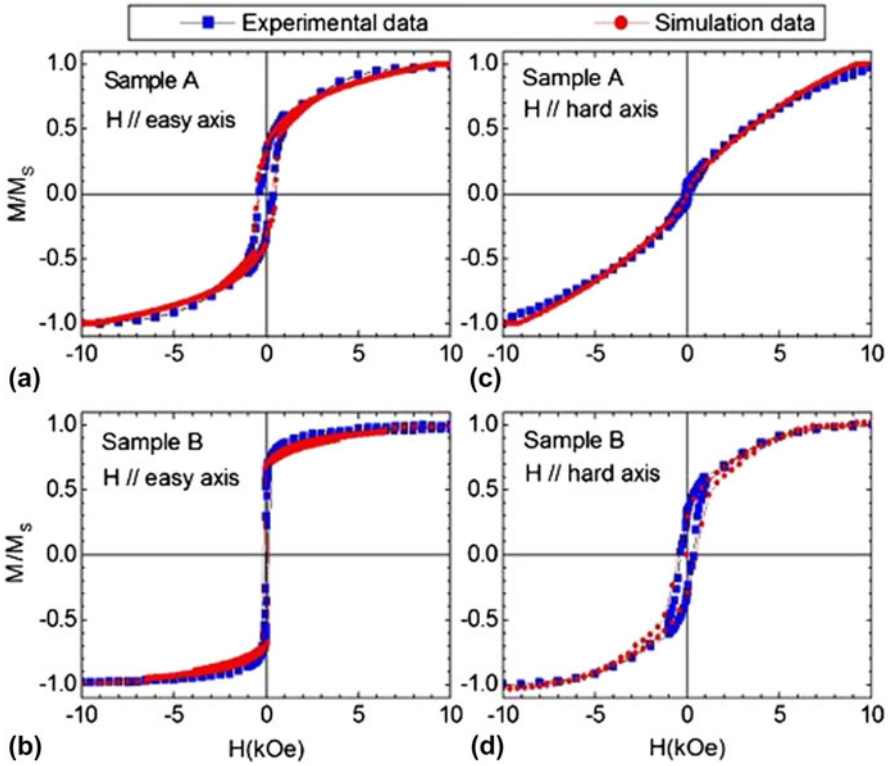

FIG. 4. Simulated (red filled circles) and experimental (blue filled squares) M–H loops for Sample A and Sample B with magnetic field applied along the easy magnetic axes in the film plane (a and b) and hard magnetic axes perpendicular to the film plane (c and d).

TABLE I. Magnetic parameters resulting from the MC simulations of magnetic hysteresis.

Sample	Axis	M_S (emu/cm^3)	K_1 (10^6 erg/cm^3)	K_2 (10^6 erg/cm^3)	H_oM_S (10^6 erg/cm^3)
A	Easy	1100	−5.02	+1.69	−3.21
	Hard	1100	−5.02	+0.64	−5.93
B	Easy	1100	−5.02	+0.85	−4.17
	Hard	1100	−5.02	+0.25	−1.33

In our simulations, the values of M_S and K_1 are kept constant and quite close to values found for bulk Co. It is noticed that the minus signal of K_1 results from the polar angle definition with respect to the film plane in our measurements. Despite the intervention of the shape anisotropy constants, K_2 values resulting from simulations are also quite reasonable if compared to values reported for bulk Co. In a certain way, it is therefore surprising that the reasonable simulations of the experimental results were obtained using a modified-SW model and considering a relatively small number of particles without dipole–dipole interactions and interparticle exchange coupling. A possible explanation to successful MC simulations is that coherent rotation of magnetization and quite uniform switching field are in fact predominant mechanisms. Furthermore, it is likely that dipole–dipole interactions have weak effective strength and conformation of the particles creates a spatial variation of the local magnetic properties, such that the intrinsic shape anisotropy and coercivity of each particle becomes efficient enough to break the interactions between particles.[23] The idea of introducing the magnetic dipolar interaction within an extension of the SW model is a very appealing goal, but very difficult indeed since the dipolar interaction is highly nonlinear. Also, the energy minimization procedure to calculate the magnetization for an applied field becomes much more complex if is taken into account the dipole–dipole interaction between particles. Dipolar interaction between particles can be made using the expression:

$$E_{\mathrm{dip}} = \sum_{i \neq j} \left(\mu_i \cdot \mu_j / {r_{ij}}^3 - 3 \left(\mu_i \cdot r_{ij} \right) \left(\mu_j \cdot r_{ij} \right) / {r_{ij}}^5 \right) \quad , \quad (3)$$

where μ_i and μ_j are the magnetic moment of the particles at sites i or j and $r_{ij} = |r_{ij}|$ is the distance between the centers of the particles. It is worth noticing that magnetic dipole–dipole interactions are directional, repulsive, or attractive depending on the relative orientation of the dipoles in the space. The dipolar energy density decays as the inverse cube of the distance between particles and scales linearly with volume of the particle. Taking the average values of particle volumes and interparticle distances, one can estimate an average dipolar energy per unit volume not exceeding $U\,(= \langle E_{\mathrm{dip}}/V_i \rangle) \sim 2 \times 10^6$ erg/cm^3. Therefore, the ratio $U/|K_1| \sim 0.4$ indicates an average dipolar interaction smaller than the first-order effective anisotropy term. Another magnetic interaction disregarded in our simulations is the interparticle exchange coupling which predominates when the ratio of surface area to volume increases with decreasing particle size.[23] Also, the interparticle exchange coupling depends on the imperfections of particle boundaries and it generally results in a decrease of exchange coupling with the disconnection of the particles.[23] Therefore, different sizes and shapes of particles, together with coercive mechanism related with spatial distribution of magnetization easy axes, contributing to the magnetic interactions play a minor role in both samples. Comparison with experimental data justifies our calculations with only a few realistic magnetic parameters.

IV. CONCLUSIONS

We developed MC simulations of the *M–H* loops based on extended SW model that take into account second-order anisotropy contribution and phenomenological nucleation for dense assemblies of magnetically noninteracting particles with variable sizes and interparticle distances. Coercive field values rather similar to experimental ones were obtained using a phenomenological nucleation energy term for magnetic particles. Our simulations reproduce quite well experimental results despite the choice of a relatively small number of magnetic particles; i.e., *M–H* loops were simulated considering only 100 particles, whereas sample sizes used in the magnetization measurements typically contain 10^6 to 10^7 particles. Indeed, the overall agreement between MC simulations and experimental data are satisfactory for assembly containing more than 100 particles, even if some discrepancies between simulated and experimental *M–H* loops are observed.

In summary, our present approach can be generalized for other systems. A relatively small number of particles were used to form a prototypal system of particles which are used to simulate a realistic system with a much larger number of individual particles. The relevance of dipole–dipole interaction between particles is not always crucial to obtain physically consistent simulations of the global magnetization of particles. In a certain way, our results demonstrate that a quite simplified extension of the SW model can be used to simulate dense assemblies of particles with nonuniform sizes, irregular distances, and distinct configurations of easy axes of magnetization. In view of the unavoidable fluctuations and deviations in size, shape, and/or intercomponent distances in many realistic self- and pattern-assembled templates of particles, the simplicity of our modeling deserves attention. Particularly, these results are important for the design and implementation of magnetic devices when noninteracting

magnetic particles are considered to store and process information.

ACKNOWLEDGMENTS

This work was supported by CNPq, SISNano, Fundação Araucária (PRONEX 17386 #118/2010) and FAPESP (2012/24025-0 and 2013/07296-2) Brazilian funding agencies.

REFERENCES

1. S. Singamanemi, V.N. Blizyiuk, C. Binek, and E.Y. Tsymbal: Magnetic nanoparticles: Recent advances in synthesis, self-assembly and applications. *J. Mater. Chem.* **21**, 16819 (2011).
2. J.L. Dormann, D. Fiorani, and E. Tronc: Magnetic relaxation in fine-particle systems. *Adv. Chem. Phys.* **98**, 283 (1997).
3. M. Bolte, R. Eiselt, G. Meier, D-H. Kim, and P. Fischer: Real space observation of dipolar interaction in arrays of Fe microelements. *J. Appl. Phys.* **99**, 08H301 (2006).
4. D.W. Abraham and Y. Lu: Observation of switching of magnetic particle arrays with dipole interaction field effects. *J. Appl. Phys.* **98**, 023902 (2005).
5. C.A. Ross, S. Haratani, F.J. Castaño, Y. Hao, M. Hwang, M. Shima, J.Y. Cheng, B. Vögeli, M. Farhoud, M. Walsh, and H.I. Smith: Magnetic behavior of lithographically patterned particles arrays. *J. Appl. Phys.* **91**, 6848 (2002).
6. C. Martinez-Boubeta, K. Simeonidis, A. Makridis, M. Angelakeris, O. Iglesias, P. Guardia, A. Cabot, L. Yedra, S. Estrade, F. Peiro, Z. Saghi, P.A. Midgley, I. Conde-Lebora, D. Serantes, and D. Baldomir: Learning from nature to improve the heat generation of iron-oxide nanoparticles for magnetic hyperthermia applications. *Sci. Rep.* **3**, 1652 (2013).
7. E.C. Stoner and E.P. Wohlfarth: A mechanism of magnetic hysteresis in heterogenous alloys. *Philos. Trans. Roy. Soc. A* **240**, 599 (1948); reprinted by *IEEE Trans. Magn.* **27**, 3475 (1991).
8. J.M. Porro, A. Berger, M. Grimsditch, V. Metlushko, B. Ilic, and P. Vavassori: Effect of spatially asymmetric dipolar interactions in the magnetization reversal of closely spaced ferromagnetic nanoisland arrays. *J. Appl. Phys.* **111**, 07B913 (2012).
9. D. Bisero, P. Cremon, M. Madami, M. Sepioni, S. Tacchi, G. Gubbiotti, G. Carlotti, A.O. Adeyeye, N. Singh, and S. Goolaup: Effect of dipolar interaction on the magnetization state of chains of rectangular particles located either head-to-tail or side-by-side. *J. Nanopart. Res.* **13**, 5691 (2011).
10. C.C. Dantas and L.A. de Andrade: Micromagnetic simulations of small arrays of submicron ferromagnetic particles. *Phys. Rev. B: Condens. Matter Mater. Phys.* **78**, 024441 (2008).
11. R. Hyndman, A. Mougin, L.C. Sampaio, J. Ferre, J.P. Jameta, P. Meyer, V. Mathet, C. Chappert, D. Mailly, and J. Gierak: Magnetization reversal in weakly coupled patterns. *J. Magn. Magn. Mater.* **240**, 34 (2002).
12. J. García-Otero, M. Porto, J. Rivas, and A. Bunde: Influence of dipolar interaction on magnetic properties of ultrafine ferromagnetic particles. *Phys. Rev. Lett.* **84**, 167 (2000).
13. T. Aign, P. Meyer, S. Lemerle, J.P. Jamet, J. Ferré, V. Mathet, C. Chappert, J. Gierak, C. Vieu, F. Rousseaux, H. Launois, and H. Bernas: Magnetization reversal in arrays of perpendicularly magnetized ultrathin dots coupled by dipolar interaction. *Phys. Rev. Lett.* **81**, 5656 (1998).
14. R.L. Stamps and R.E. Camley: High-frequency response and reversal dynamics of two-dimensional magnetic dot array. *Phys. Rev. B: Condens. Matter Mater. Phys.* **60**, 12264 (1999).
15. M.R. Scheinfein, K.E. Schmidt, K.R. Heim, and G.G. Hembree: Magnetic order in two-dimensional arrays of nanometer-sized superparamagnets. *Phys. Rev. Lett.* **76**, 1541 (1996).
16. H-F. Du, W. He, D-L. Sun, Y-P. Fang, H-L. Liu, X-Q. Zhang, and Z-H. Chen: Monte Carlo simulation of magnetic properties of irregular Fe islands on Pb/Si(111) substrate based on the scanning tunneling microscopy image. *Appl. Phys. Lett.* **96**, 132502 (2010).
17. J. Varalda: Caracterização magnética de filmes de ligas e multicamadas magnéticas (in portuguese). M. Sc. Thesis, Universidade Federal de São Carlos, 2000.
18. O. Karaagac, H. Kockar, and M. Alper: Electrodeposited cobalt films: The effect of deposition potentials on the film properties. *J. Optoelectron. Adv. Mater.* **15**, 1412 (2013).
19. Z. Szabó and A. Iványi: Computer-aided simulation of Stoner-Wohlfarth model. *J. Magn. Magn. Mater.* **215**, 33 (2000).
20. M. Jamet, W. Wernsdorfer, C. Thirion, V. Dupuis, P. Melinon, and A. Perez: Magnetic anisotropy in single clusters. *Phys. Rev. B: Condens. Matter Mater. Phys.* **69**, 024401 (2004).
21. V.Z.C. Paes, I.L. Graff, J. Varalda, V.H. Etgens, and D.H. Mosca: The role of magnetoelastic and magnetostrictive energies in the magnetization process of MnAs/GaAs epilayers. *J. Phys.: Condens. Matter* **25**, 046003 (2013).
22. D-X. Chen, E. Pardo, and A. Sanchez: Demagnetizing factors of rectangular prisms and ellipsoids. *IEEE Trans. Magn.* **38**, 1742 (2002).
23. H-W. Zhang, S-Y. Zhang, B-G. Shen, and H. Kronmuller: The magnetization behavior of nanocrystalline permanent magnets based on the Stoner–Wohlfarth model. *J. Magn. Magn. Mater.* **260**, 352 (2003).
24. A. Winter, H. Pascher, H. Krenn, X. Liu, and J.K. Furdyna: Interpretation of hysteresis loops of GaMnAs in the framework of the Stoner–Wohlfarth model. *J. Appl. Phys.* **108**, 043921 (2010).
25. D. Hrabovsky, E. Vanelle, A.R. Fert, D.S. Yee, J.P. Redoules, J. Sadowski, J. Kanski, and L. Ilver: Magnetization reversal in GaMnAs layers studied by Kerr effect. *Appl. Phys. Lett.* **81**, 2806 (2002).
26. R. Skomski, G.C. Hadjipanayis, and D.J. Sellmyer: Effective demagnetizing factors of complicated particle mixtures. *IEEE Trans. Magn.* **43**, 2956 (2007).